



1 **A regional spatio-temporal analysis of large magnitude** 2 **snow avalanches using tree rings**

3 Erich Peitzsch^{1,2*}, Jordy Hendrikx², Daniel Stahle¹, Gregory Pederson¹, Karl Birkeland^{3,2},
4 and Daniel Fagre¹

5 ¹ U.S. Geological Survey Northern Rocky Mountain Science Center, West Glacier, Montana, USA

6 ² Snow and Avalanche Lab, Department of Earth Sciences, Montana State University, Bozeman, Montana,
7 USA

8 ³ U.S.D.A. Forest Service National Avalanche Center, Bozeman, Montana, USA

9 *epeitzsch@usgs.gov, 215 Mather Dr., West Glacier, MT, USA, 59936

10 **Abstract.** Snow avalanches affect transportation corridors and settlements worldwide. In many mountainous
11 regions, robust records of avalanche frequency and magnitude are sparse or non-existent. However,
12 dendrochronological methods can be used to fill this gap and infer historic avalanche patterns. In this study,
13 we developed a tree-ring based avalanche chronology for large magnitude avalanche events using
14 dendrochronological techniques for a portion of the northern United States Rocky Mountains. We used a
15 strategic sampling design to examine avalanche activity through time and across nested spatial scales (i.e.
16 from individual paths, four distinct sub-regions, and the region). We analysed 673 total samples from 647
17 suitable trees collected from 12 avalanche paths, from which 2,134 growth disturbances were identified over
18 years 1636 to 2017 Common Era (C.E.). Using existing indexing approaches, we developed a regional
19 avalanche activity index to discriminate avalanche events from noise in the tree-ring record. Large magnitude
20 avalanches common across the region occurred in 30 individual years and exhibited a median return interval
21 of approximately three years (mean = 5.21 years). The median large magnitude avalanche return interval (3-
22 8 years) and the total number of avalanche years (12-18) vary throughout the four sub-regions, suggesting
23 the important influence of local terrain and weather factors. We tested subsampling routines for regional
24 representation, finding that sampling eight random paths out of a total of 12 avalanche paths in the region
25 captures up to 83% of the regional chronology, whereas four paths capture only 43% to 73%. The greatest
26 value probability of detection for any given path in our dataset is 40% suggesting that sampling a single path
27 would capture no more than 40% of the regional avalanche activity. Results emphasize the importance of
28 sample size, scale, and spatial extent when attempting to derive a regional large magnitude avalanche event
29 chronology from tree-ring records.

30



31 **1 Introduction**

32 **1.1 Background**

33 Snow avalanches are hazardous to human safety and infrastructure (Mock et al., 2016; Schweizer, 2003) as
34 well as an important landscape disturbance affecting mountain ecosystems (Bebi et al., 2009). In the United
35 States an average of 27 people die in avalanche accidents each winter (CAIC, 2020). Avalanches, especially
36 large magnitude events, also affect transportation corridors and settlements throughout the world. For
37 example, avalanches impact numerous roadways and railroad corridors in the western United States
38 (Armstrong, 1981; Hendrikx et al., 2014; Reardon et al., 2008). Consequently, understanding general
39 avalanche processes and associated large magnitude avalanche return intervals is critical for local and
40 regional avalanche forecasters, transportation agencies, and land use planners.

41 Long-term, reliable, and consistent avalanche observation records are necessary for calculating avalanche
42 return intervals which can be used in infrastructure planning and avalanche forecasting operations. However,
43 such records are often sparse or non-existent in many mountainous regions, including areas with existing
44 transportation corridors. Thus, inferring avalanche frequency requires the use of dendrochronological
45 methods to document damaging events or geomorphic response within individual trees at individual path to
46 regional scales. Even in regions with historical records, tree-ring dating methods can be used to extend or
47 validate uncertain historical avalanche records, which has led to the broad implementation of these methods
48 in mountainous regions throughout the world (e.g. Corona et al., 2012; Favillier et al., 2018; Schläppy et al.,
49 2014).

50 Numerous studies reconstructed avalanche chronologies in the United States using tree-ring methods
51 (Burrows and Burrows, 1976; Butler et al., 1987; Carrara, 1979; Hebertson and Jenkins, 2003; Potter, 1969;
52 Rayback, 1998;). Butler and Sawyer (2008) provided a review of current methodologies and types of tree-
53 ring responses used in avalanche dendrochronological studies. Favillier et al. (2018) provided a more recent
54 comprehensive graphical summary of dendrochronological avalanche studies throughout the world.
55 Numerous studies used dendrochronological techniques to develop avalanche chronologies for remote
56 regions without historical avalanche records or areas with inconsistent avalanche observations (Butler and
57 Malanson, 1985a; Germain et al., 2009; Reardon et al., 2008; Šilhán and Tichavský, 2017; Voiculescu et al.,
58 2016), and many studies used these techniques to examine avalanches across space and time (Table 1).

59



60 **Table 1: List of previous avalanche-dendrochronological work with more than one avalanche path in study – to**
 61 **place our regional work in context with other regional/multiple path studies. Number of samples, paths, growth**
 62 **disturbances (GD), and spatial extent (linear distance between most distant avalanche paths in study area) are**
 63 **included. For spatial extent, NA is reported in studies where spatial extent is not reported or could not be inferred**
 64 **from maps in the published work. Where spatial extent is not reported directly in previous work, it is estimated**
 65 **by using maps from the published work and satellite imagery.**

Authors	Location	# Trees	# Samples	# Paths	Spatial Extent	# GD
Gratton et al. (2019)	Northern Gaspé Peninsula, Québec, Canada	82	177 cores 65 x-sec	5	~20 km	Not provided
Meseşan et al. (2018)	Parâng Mountains, Carpathians, Romania	232	430 cores 39 x-sec 4 wedges	3	~16 km	Not provided
Favillier et al. (2018)	Zermatt valley, Switzerland	307	620 cores 60 x-sec	3	~1 km	2570
Ballesteros-Canovas (2018)	Kullu district, Himachal Pradesh, India	114	Not Provided	1 slope (multiple paths)	~1 km	521
Pop et al. (2018)	Piatra Craiului Mountains, Romania	235	402 cores 34 x-sec	2	~2 km	789
Martin and Germain (2016)	White Mountains, New Hampshire	450	350 cores 456 x-sec	7	~10 km	2251
Voiculescu et al. (2016)	Făgăras massif, Carpathians, Romania	293	586 cores	4	NA	853
Schläppy et al. (2015)	French Alps, France	967	1643 cores 333 x-sec	5	~100 km	3111
Schläppy et al. (2014)	French Alps, France	297	375 cores 63 x-sec	2	~100 km	713
Schläppy et al. (2013)	French Alps, France	587	1169 cores 122 x-sec	3	~100 km	1742
Casteller et al. (2011)	Santa Cruz, Argentina	95	~95 x-sec	9	~2 km	Not provided
Köse et al. (2010)	Katsomonu, Turkey	61	Not provided	2	~500 m	Not provided



Muntán et al. (2009)	Pyrenees, Catalonia	NA	448	6	~150 km	Not provided
Germain et al. (2009)	Northern Gaspé Peninsula, Québec, Canada	689	1214 x-sec	12	~30 km	2540
Butler and Sawyer (2008)	Lewis Range, Glacier National Park, Montana, USA	22	22 x-sec	2	~5 km	Not provided
Casteller et al. (2007)	Grisons, Switzerland	145	122 x-sec 52 cores 10 wedges	2	~ 20 km	Not provided
Germain et al. (2005)	Northern Gaspé Peninsula, Québec, Canada	142	142 x-sec	5	NA	420
Dube et al. (2004)	Northern Gaspé Peninsula, Québec, Canada	110	170 x-sec	3	~9 km	Not provided
Hebertson and Jenkins (2003)	Wasatch Plateau, Utah, USA	261	Not provided	16	NA	Not provided
Rayback (1998)	Front Range, Colorado, USA	98	58 trees cored (2-5 cores /tree) 31 x-sec 9 wedges	2	~7 km	Not provided
Bryant et al. (1989)	Huerfano Valley, Colorado, USA	180	Not provided	3	~2 km	Not provided
Butler and Malanson (1985a)	Lewis Range, Glacier National Park, Montana, USA	78	Not provided	2	~6 km	Not provided
Butler (1979)~	Glacier National Park, Montana, USA	NA	36 x-sec 17 cores	12	~15 km	Not provided
Smith (1973)	North Cascades, Washington, USA	NA	Not provided	11	~ 35 km	Not provided
Potter (1969)	Absaroka Mountains, Wyoming, USA	50	Not provided	5	~ 2 km	50



67 1.2 Framework and objectives

68 Tree-ring avalanche research is resource and time intensive. Like other scientific fields, it is not feasible to
69 completely sample the variable of interest with infinite detail due to logistical and financial constraints
70 (Skøien and Blöschl, 2006). Thus, a strategic spatial sampling method is necessary. Here, we strategically
71 sampled 12 avalanche paths in four distinct sub-regions of the U.S. northern Rocky Mountains of northwest
72 Montana to examine spatial differences at a regional scale. The sampling strategy is based on the concept of
73 scale triplet, which defines the spacing, extent, and support of our sampling scheme (Blöschl and Sivapalan,
74 1995). Incorporating the scale triplet concept helps us understand the nature of the problem, the scale at which
75 measurements should be made, and how we can estimate the measurements across space. Often, the scale at
76 which samples are collected differs from the scale necessary for predictive purposes (Blöschl, 1999). For
77 example, if we are interested in avalanche frequency relationships with regional climate patterns but tree-
78 ring samples are collected at an avalanche path scale, then a network of sampled paths need to be spaced and
79 aggregated across the core of the climatically similar region. In our study, the extent is the entire region and
80 sub-regions, the spacing is the distance between avalanche paths and sub-regions, and the support is the size
81 of the area being sampled. In addition, the process scale is the natural variability of avalanche frequency, the
82 measurement scale is the tree-ring proxies used to represent avalanche occurrence on an annual temporal
83 scale, and the model scale relates to aggregating all of the sample areas to derive a regional avalanche
84 chronology.

85 We adopt Germain's (2016) definition that large magnitude avalanches are events characterized by low and
86 variable frequency with a high capacity for destruction. This generally translates to a size 3 or greater on the
87 destructive classification scale - i.e. ability to bury or destroy a car, damage a truck, destroy a wood frame
88 house, or break a few trees (Greene et al., 2016).

89 Understanding the spatiotemporal behavior of large magnitude avalanches on the regional scale will improve
90 avalanche forecasting efforts, especially for operations involving avalanche terrain that impacts
91 transportation corridors. Here, we aim to answer three specific questions:

- 92 1) What is the regional, sub-regional, and path specific frequency of large magnitude avalanches in the U.S.
93 northern Rocky Mountains of northwest Montana?
- 94 2) How does the spatial extent of the study region affect the resultant avalanche chronology?
- 95 3) What is the probability of detecting regional avalanche activity by sampling different avalanche paths?

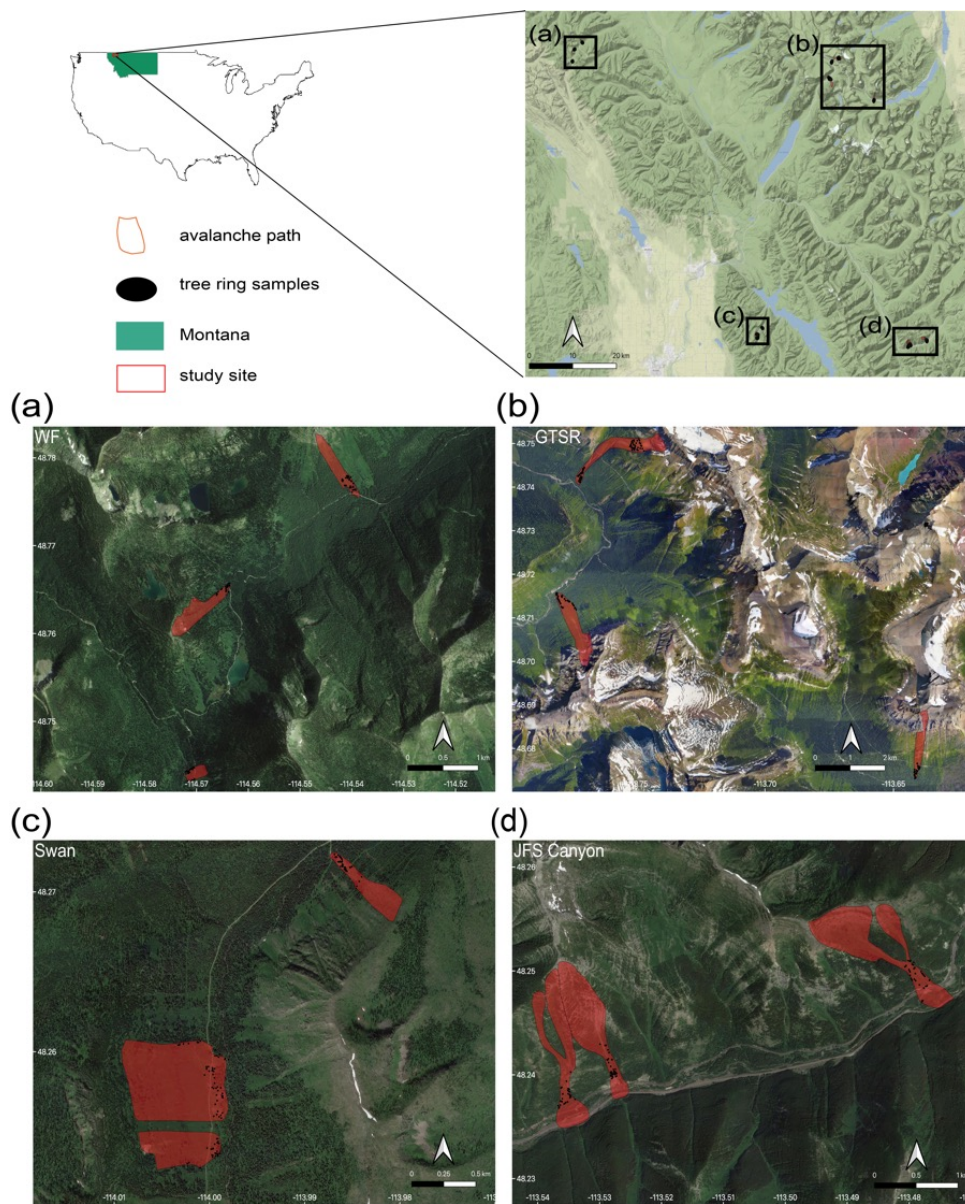
96 To our knowledge, this is the first study to look at how various spatial scales compare when reconstructing a
97 regional avalanche chronology from dendrochronological data on a large dataset ($N > 600$ samples). Further,
98 we believe this is the first study that utilizes a regional dendrochronological record to derive return periods
99 over a large ($> 3000 \text{ km}^2$) spatial extent. Our hypothesis is that aggregating the paths into sub-region and
100 then again into a full region allows us to minimize the limitation of tree-ring avalanche chronologies
101 underestimating avalanche years at these scales.



102 **2. Methodology**

103 **2.1 Study Site**

104 Our study site consists of 12 avalanche paths in the Rocky Mountains of northwest Montana, USA (Figure 1
105 and Table 2). We sampled sets of three avalanche paths in four distinct sub-regions within three mountain
106 ranges: the Whitefish Range (WF, Red Meadow Creek) and Swan Range (Swan, Lost Johnny Creek) on the
107 Flathead National Forest, and two sub-regions within the Lewis Range in Glacier National Park (GNP),
108 Montana. The sites in GNP are along two major transportation corridors through the park: the Going-to-the-
109 Sun Road (GTSR) and U.S. Highway 2 in John F. Stevens (JFS) Canyon. These two areas were utilized for
110 previous dendrochronological avalanche research (Butler and Malanson, 1985a; Butler and Malanson,
111 1985b; Butler and Sawyer, 2008; Reardon et al., 2008). A robust regional avalanche chronology
112 reconstruction will help place the previous work in context of the wider region. The other two sites, WF and
113 Swan, are popular backcountry recreation areas with access via snowmachine in the winter along a U.S.
114 Forest Service road. The avalanche paths in each sub-region encompass a range of spatial extents from
115 adjacent (i.e. < 30 m apart) to ~10 km apart. Overall, this study region provides an ideal natural setting for
116 studying avalanches due to its geography, inclusion of transportation and recreation corridors potentially
117 impacted by avalanches, relative accessibility, and no artificial avalanche hazard mitigation.



118

119 **Figure 1: Study site.** The red rectangle in the state of Montana designates the general area of the four sampling
120 sites. The sites are (A) Red Meadow, Whitefish Range (WF), (B) Going-to-the-Sun Road (GTSR), central GNP,
121 (C) Lost Johnny Creek, northern Swan Range (Swan), and (D) John F. Stevens Canyon (JFS), southern GNP.
122 Satellite and map imagery: © Google (n.d.). Maps produced using ggmap in R (Korpela et al. 2019).

123



124 **Table 2: Topographic characteristics of all avalanche paths. Different colors indicate sub-regions as shown in**
 125 **Figure 1. * denotes two major starting zones for one runout in Shed 10-7 and Shed 7 paths.**

Path	n	Full Path Elev. (mean) (m)	Full Path Elev. (range) (m)	Starting Zone Elev. (mean) (m)	Full Path Slope (mean) (°)	Starting Zone Slope (mean) (°)	Median Aspect (°)	Area (km ²)	Length (m)	Vertical (m)	Years of previous fire or logging
WF-Red Meadow A (RMA)	41	1651	1462 - 1957	1774	26	32	155	0.32	1004.97	495.20	1952
WF-Red Meadow B (RMB)	40	1870	1643 - 2164	1965	31	37	53	0.13	1041.98	521.27	1967
WF-Red Meadow C (RMC)	42	1650	1582 - 1742	1692	28	33	257	0.08	326.14	160.46	1962
GTSR - 54-3	56	1501	1080 - 2149	1708	31	40	327	0.44	2063.61	1068.49	NA
GTSR-Little Granite (LGP)	109	1770	1109 - 2314	2170	24	34	250	0.78	2940.29	1205.07	NA
GTSR-Jackson Glacier Overlook (JGO)	41	1863	1500 - 2660	2090	32	42	180	0.70	1793.13	1159.84	NA
Swan-Lost Johnny A (LJA)	53	1619	1441 - 1896	1731	29	38	77	0.41	811.50	455.27	1971-72
Swan-Lost Johnny B (LJB)	26	1633	1478 - 1879	1721	32	39	76	0.57	617.52	401.80	1971-72
Swan-Lost Johnny C (LJC)	42	1550	1344 - 1750	1670	34	36	326	0.39	667.88	405.66	1957, 2003
JFS-Shed 10-7 (S10.7)*	109	1644	1233 - 2193	1910 - 1964	31	35 - 39	176	0.13	1745.66	959.74	1910
JFS-Shed 7 (S7)*	46	1712	1310 - 2078	1935 - 1837	29	34 - 36	152	0.57	1686.96	768.01	1910
JFS-1163	50	1718	1250 - 2217	1861	38	42	158	0.17	1636.52	966.82	1910
All Paths	655	1690	1080 - 2660	1869	-0.17	0.14	31	37	Spatial footprint = 3500 km ²		

126



127 Northwest Montana's avalanche climate is classified as both a coastal transition and intermountain avalanche
128 climate (Mock and Birkeland, 2000), but it can exhibit characteristics of both continental or coastal climates.
129 The elevation of avalanche paths within the study sites range from approximately 1100 m to 2700 m and the
130 starting zones of these paths are distributed among all aspects (Table 2).

131 We eliminated or minimized influence from exogenous disturbance factors such as logging and wildfire by
132 referencing wildfire maps extending back to the mid-20th century. We selected sites undisturbed by wildfire
133 since this time except for Lost Johnny Creek, which was purposeful as this area burned most recently in 2003.
134 We also minimized the influence of logging by selecting sites not previously logged. Using historical logging
135 parcel spatial data, we determined logging in some sites was limited to very small parcels adjacent to the
136 farthest extent of the runout zones.

137 The historical observational record in this area is limited. In this study region, the Flathead Avalanche Center
138 (FAC), a regional U.S. Forest Service backcountry avalanche center, records all avalanches observed and
139 reported to the center. However, not all avalanches are observed or reported given the approximately 3500
140 km² advisory area. The Burlington-Northern Santa Fe Railway (BNSF) Avalanche Safety Program records
141 most avalanches observed in John F. Stevens Canyon in southern Glacier National Park, where there is 16
142 km of rail line with over 40 avalanche paths. However, systematic operational observations only began in
143 2005. Observations prior to this time are inconsistent, though large magnitude avalanches were mostly
144 recorded. Reardon et al. (2008) developed as complete a record as possible from the Department of
145 Transportation and railroad company records, National Park Service ranger logs, and popular media archives.
146 In this sub-region avalanche mitigation is conducted on an infrequent and inconsistent basis in emergency
147 situations, which is typically only once a year, if at all. Thus, the record approximates a natural avalanche
148 record. We compared the reconstructed avalanche chronology of the JFS sub-region to the historical record
149 for qualitative purposes of large magnitude years. A quantitative comparison would not be reflective of the
150 true reliability of tree-ring methods because of the incomplete historical record.

151 **2.2 Sample Collection and Processing**

152 Our sampling strategy targeted an even number of samples collected from both lateral trimlines at varying
153 elevations and trees located in the main lower track and runout zone of the selected avalanche paths. This
154 adequately captured trees that were destroyed and transported, as well as those that remained in place.

155 Sample size for avalanche reconstruction using tree-ring data requires careful consideration. Butler and
156 Sawyer (2008) suggest that a few damaged trees may be sufficient for avalanche chronologies, but larger
157 target sample sizes increase the probability of detecting avalanche events (Corona et al., 2012). Germain et
158 al. (2010) examined cumulative distribution functions of avalanche chronologies and reported only slight
159 increases in the probability of extending chronologies with sample size greater than 40. Thus, given the large
160 spatial footprint (~3500 km²) of this study and feasibility of such a large sample size, we sampled between
161 26-109 samples per avalanche path resulting in 655 trees (Table 2). Eight trees were unsuitable for analysis
162 leaving us with 673 total samples from 647 trees. Of the 673 total samples, we collected 614 cross sections



163 and 59 cores. Shed 10.7 (S10.7) path was the focus of previous work (Reardon et al., 2008), and the
164 dendrochronological record extends up to 2005 (n=109 trees). Little Granite Path (LGP) was collected in the
165 summer of 2009 (n=109 trees). We sampled the remaining 10 paths (437 of the 655 total trees) in the summer
166 of 2017.

167 We collected full stem cross-sections from dead (both downed and standing dead) trees, and cores from live
168 trees. We used predominantly cross-sections in this study for a more robust analysis as events can potentially
169 be missed or incorrectly identified in cores. We emphasized the selection of trees with obvious external scars
170 and considered location, size, and potential age of tree samples. A limitation of all avalanche
171 dendrochronology studies is that large magnitude events cause extensive damage and high tree mortality,
172 thereby reducing subsequent potential tree-ring records.

173 We sampled stem cross-sections at the location of an external scar or just above the root buttress from downed
174 or standing and dead trees, and from stumps of trees topped by avalanche damage. We extracted tree-ring
175 core samples from live trees with obvious scarring or flagging along the avalanche path margins and runoff
176 zone using a 5 mm diameter increment borer. We collected a minimum of two and up to four core samples
177 per tree (two in the uphill-downhill direction and two perpendicular to the slope). We photographed each
178 sample at each location and recorded species, GPS coordinates (accuracy 1-3 m), amount of scarring on the
179 cambium of the tree, relative location of the tree in the path, and upslope direction (Peitzsch et al., 2019). We
180 also recorded location characteristics that identified the tree to be in-place vs. transported from its original
181 growth position (i.e. presence or absence of roots attached to the ground or the distance from an obvious
182 excavated area where the tree was uprooted).

183 To prevent radial cracking and further rot, we dried and stabilized the cross sections with a canvas backing.
184 We sanded samples using a progressively finer grit of sandpaper to expose the anatomy of each growth ring,
185 and used the visual skeleton plot method to account for missing and false-rings and for accurate calendar
186 year dating (Stokes and Smiley, 1996). We assessed cross-dating calendar-year accuracy of each sample and
187 statistically verified against measured samples taken from trees within the gallery forest outside the avalanche
188 path, and from preexisting regional chronologies (Table A1) (ITRDB, 2018) using the dating quality control
189 software COFECHA (Grissino-Mayer, 2001;Holmes, 1983). For further details on cross-dating methods and
190 accuracy calculation for this dataset see Peitzsch et al. (2019).

191 **2.3 Avalanche Event Identification**

192 We analyzed samples for signs of traumatic impact events (hereafter “responses”) likely caused by snow
193 avalanches. We adapted a classification system from previous dendrogeomorphological studies to
194 qualitatively rank the trauma severity and tree growth response from avalanche impacts using numerical
195 scores ranked 1 through 5 (Reardon et al., 2008). This classification scheme identified more prominent
196 avalanche damage responses with higher quality scores, and allowed us to remain consistent with previous
197 work (Corona et al., 2012; Favillier et al., 2018) (Table 3). To compare our ability to capture avalanche /
198 trauma events using cores versus those captured using cross-sections, we sampled a subset (n=40) of the



199 cross-sections by analyzing four 5 mm wide rectangles to mimic a core sample from an increment borer. The
 200 four subsamples on each cross section were made perpendicular to one another (i.e. 90 degrees) based on the
 201 first sample taken from the uphill direction of each stem to replicate common field sampling methods. We
 202 then summarized results from the four subsamples for each tree by taking the highest response score for each
 203 growth year. Finally, we compared the number, quality response category, and calendar year of the avalanche
 204 / trauma events derived from the core subsamples to those identified from the full cross sections.

205

206 **Table 3: Avalanche impact trauma classification ratings.**

Classification	Description
C ₁	<ul style="list-style-type: none"> • Clear impact scar associated with well-defined reaction wood, growth suppression or major traumatic resin duct development. • Or, the strong presence of some combination of these major anatomical markers of trauma and growth response recorded in multiple years of growth and occurring at a year that multiple samples from other trees at the site record similar trauma and scarring. • C₁ events are also assigned to the death date of trees killed by observed avalanche mortality at the collection site; the presence of earlywood indicates an early spring, or late avalanche season, event killed the tree.
C ₂	<ul style="list-style-type: none"> • Scar or small scar recorded in the first ten years of tree growth without associated reaction wood, growth suppression or traumatic resin ducts. • Or, obvious reaction wood, growth suppression or significant presence of traumatic resin ducts that occur abruptly after normal growth that lasts for 3 or more years.
C ₃	<ul style="list-style-type: none"> • The presence of reaction wood, growth suppression, or traumatic resin ducts recorded in less than 3 successive growth years.
C ₄	<ul style="list-style-type: none"> • Poorly defined reaction wood, growth suppression or minimal presence of traumatic resin ducts lasting 1-2 years. • Or, a C₃ class event occurring in the first 10 years of tree growth where the cause of damage could result from various biological and environmental conditions.
C ₅	<ul style="list-style-type: none"> • Very poorly defined reaction wood, growth suppression, or minimal presence of traumatic resin ducts isolated in one growth year. • Or, a C₄ class event occurring in the first 10 years of tree growth where the cause of damage could result from various biological and environmental conditions.

207



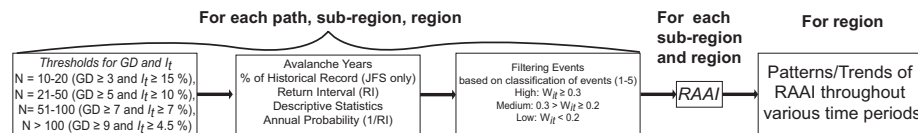
208 **2.4 Chronology and Return Period Calculation**

209 To generate avalanche event chronologies and estimate return periods for each path and for the entire study
 210 site, we utilized *R* statistical software and the package *slideRun*, an extension of the *burnR* library for forest
 211 fire history data (Malevich et al., 2018). We calculated the age of each tree sampled and the number of
 212 responses per year and computed descriptive statistics for the entire dataset. Estimates of avalanche path
 213 return intervals should be viewed as maximum return interval values due to the successive loss of samples
 214 and decreasing sample number back through time.
 215 We used a multi-step process to reconstruct avalanche chronologies on three different spatial scales:
 216 individual paths, four sub-regions, and the entire region. We also calculated a regional avalanche activity
 217 index (RAAI) (Figure 2). The process involved first calculating the ratio of trees exhibiting GD over the
 218 number of samples alive at year *t* to provide the index *I_t* (Shroder, 1978):

$$I_t = \left(\frac{\sum_{i=1}^n (R_t)}{\sum_{i=1}^n (A_t)} \right) \times 100 \quad (1)$$

219 where *R* is the number of trees recording a GD at year *t* with *A_t* representing the number of trees alive in our
 220 samples at year *t*.

221



222

223 **Figure 2: General workflow of analytical methods to reconstruct regional avalanche chronology and regional**
 224 **avalanche activity index.**

225 We then used double thresholds to estimate the minimum absolute number of GD and a minimum percentage
 226 of samples exhibiting GD per year (*I_t*) based on sample size following thresholds established by Corona et
 227 al. (2012) and Favillier et al. (2018): *N* = 10-20 (*GD* ≥ 3 and *I_t* ≥ 15 %), *N* = 21-50 (*GD* ≥ 5 and *I_t* ≥ 10 %),
 228 *N* = 51-100 (*GD* ≥ 7 and *I_t* ≥ 7 %), and *N* > 100 (*GD* ≥ 9 and *I_t* ≥ 4.5 %). We then estimated the number of
 229 avalanche years, descriptive statistics for return intervals (RI), and the annual probability (1/RI) for each
 230 path, sub-region, and region.

231 We used the chronologies derived from this process to calculate a weighted index factor (*W_{it}*). We used this
 232 established threshold approach since it has been broadly employed in the literature and allows comparability
 233 of our avalanche chronology to results reported in other studies. We adapted previous equations of a weighted
 234 response index (Kogelnig-Mayer et al., 2011) to our 5-scale ranking quality classification to derive the *W_{it}*:

$$W_{it} = \left(\left(\sum_{i=1}^n T_{C_1} * 7 \right) + \left(\sum_{i=1}^n T_{C_2} * 5 \right) + \left(\sum_{i=1}^n T_{C_3} * 3 \right) + \left(\sum_{i=1}^n T_{C_4, C_5} \right) \right) * \frac{\sum_{i=1}^n R_t}{\sum_{i=1}^n A_t} \quad (2)$$

235 where the sum of trees with scars or injuries (*C₁* - *C₅*) were multiplied by a factor of 7, 5, 3, 1 and 1
 236 respectively (Kogelnig-Mayer et al., 2011).



237 Next, we classified W_{it} into high, medium, and low confidence events using the thresholds detailed in Favillier
238 et al. (2018), where High: $W_{it} \geq 0.3$, Medium: $0.3 > W_{it} \geq 0.2$, Low: $W_{it} < 0.2$. This provided another step
239 discriminating the avalanche events/years signal from noise. We included all events with medium to high
240 confidence in the next analysis. For this subset of higher-quality events, we calculated the number of
241 avalanche years, descriptive statistics for return intervals, and annual probability for each avalanche path,
242 sub-region, and overall region. We then compared return intervals for all individual paths and sub-regions
243 using analysis of variance (ANOVA) and Tukey's Honest Significant Difference (HSD) (Ott and
244 Longnecker, 2016).

245 Next, we compared the number of avalanche years and return periods identified in the full regional
246 chronology to subsets of the region to determine the number of paths required to replicate a full 12-path
247 regional chronology. We assessed the full chronology against a subsampling of 11 total paths by sequentially
248 removing the three paths with the greatest sample size. We then randomly sampled two paths from each sub-
249 region for a total subsample of eight paths, followed by generating a subsample of four paths by choosing
250 the path in each sub-region with the greatest sample size. Finally, we selected a random sample of one path
251 from each sub-region to compare against a total of four single path subsamples.

252 2.5 Regional Avalanche Activity Index and Probability of Detection

253 Next, we used the I_t statistic from each path to calculate a regional avalanche activity index (RAAI) for the
254 sub-regions and overall region (Germain et al., 2009). The RAAI for each year across the sub-regions and
255 region provides a more comprehensive assessment of avalanche activity within the spatial extent. For each
256 year t , we calculated RAAI:

$$RAAI_t = \left(\sum_{i=1}^n I_t \right) / \left(\sum_{i=1}^n P_t \right) \quad (3)$$

257 where I is the index factor as per Eq. (1) for a given avalanche path for year t and P is the number of paths
258 that could potentially record an avalanche for year t . For the calculation of the overall RAAI, we required
259 each path to retain a minimum sample size of ≥ 10 trees with a minimum number of three paths for year t ,
260 and a minimum of one path from each sub-region. We performed a sensitivity test to establish the minimum
261 number of paths necessary to calculate an RAAI value for any given year.

262 We also calculated the probability of detecting an avalanche year identified in the regional chronology as if
263 any given individual path was sampled. The probability of detection for a given year (POD_{year}) is defined as:

$$POD_{year} = \frac{a}{a + b} \quad (4)$$

264 where a is the number of individual avalanche paths that identify any given avalanche year in the regional
265 chronology and b is the total number of avalanche paths ($n=12$). We calculated POD_{year} for every year in the
266 regional avalanche chronology. We then compared the POD_{year} of individual paths to the number of active
267 avalanche paths as defined in Eq. (3).

268 We also calculated the probability of detection for each path for the period of record (POD_{path}):



$$POD_{path} = \frac{c}{c + d} \quad (4)$$

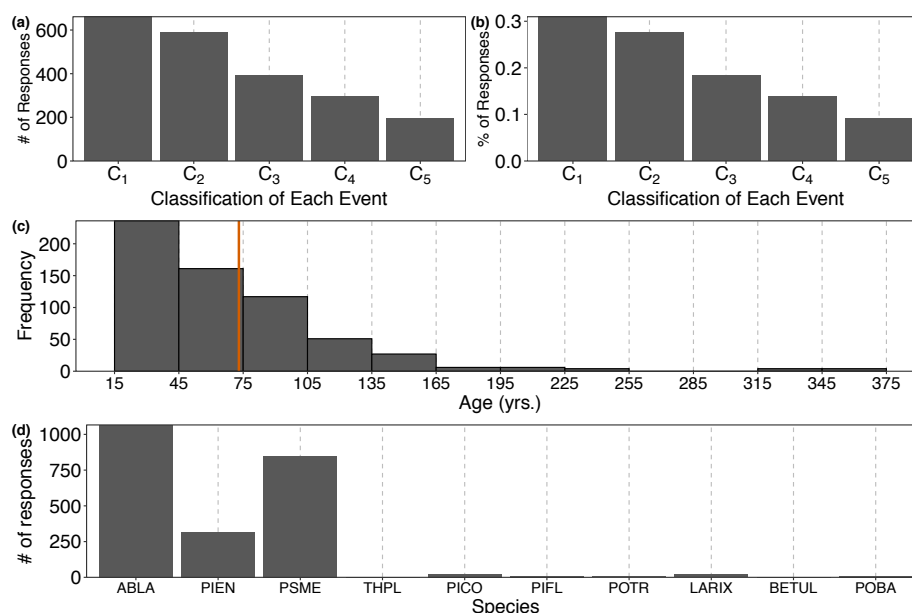
269 where c is the number of years identified in any given path that is included in the regional chronology and d
270 is the number of years in the regional chronology that are not identified in the chronology for the given path.
271 Finally, we examined trends in the RAAI through time using the non-parametric modified Mann-Kendall test
272 for trend (Mann, 1945; Hamed and Rao, 1998). We parsed the dataset into four periods to allow comparability
273 due to the loss of evidence and a decreasing sample size going back in time: the entire period of record, 1933
274 to 2017, 1950 to 2017, and 1990 to 2017. We selected these time periods based on the years with greatest
275 responses and peak RAAI values (1933, 1950, and 1990). We excluded intervals after 1990 to retain a
276 minimum of ~30-year record.

277 2.6 Geomorphological characteristics

278 Using a 10 m digital elevation model (DEM), we calculated a number of geomorphological characteristics
279 for each path, including mean elevation (m, full path and starting zone), elevation range (m), eastness
280 ($\sin(\text{aspect})$) and northness ($\cos(\text{aspect})$) (radians), slope (degrees, full path and starting zone), curvature
281 (index (0-1), profile and planform), roughness (index, full path and starting zone), perimeter (km²), area
282 (km²), length (m), and vertical distance from starting zone to runout zone (m). We also calculated the mean
283 of these characteristics for all paths in the region. The geomorphological characteristics allowed for a
284 determination of the representativeness of the region as a whole (i.e. are the paths similar across the region?)
285 as well as a comparison of the return interval for each path relative to these characteristics. Finally, we
286 estimated the potential relationship between path length, starting zone slope angle, the number of avalanche
287 years, and median return interval for each individual path using the Pearson correlation coefficient.

288 3. Results

289 We collected a total of 673 samples from 647 suitable avalanche impacted or killed trees in the full 12-path
290 regional avalanche collection. Of those 673 samples, 614 were cross sections (91%) and 59 were cores (9%).
291 Within these samples we identified 2134 GD, of which 1279 were classified as C_1 and C_2 (60%) (Figure 3(a
292 and b)). The oldest individual tree sampled was 367 years, and the mean age of all samples was 73 years
293 (Figure 3(c)). The period of record of sampled trees extended from 1636 to 2017 C.E. The most common
294 species in our dataset was *Abies lasiocarpa* (ABLA, sub-alpine fir) (46%) followed by *Pseudotsuga menziesii*
295 (*PSME*, Douglas-fir) (37%) and *Picea engelmannii* (*PIEN*, Engelmann spruce) (14%) (Figure 3(d)). The
296 oldest GD response dates to year 1655. In the entire dataset, the five years with the greatest number of raw
297 GD responses were 2002 (165 responses), 2014 (151 responses), 1990 (93 responses), 1993 (90 responses),
298 and 1982 (75 responses).

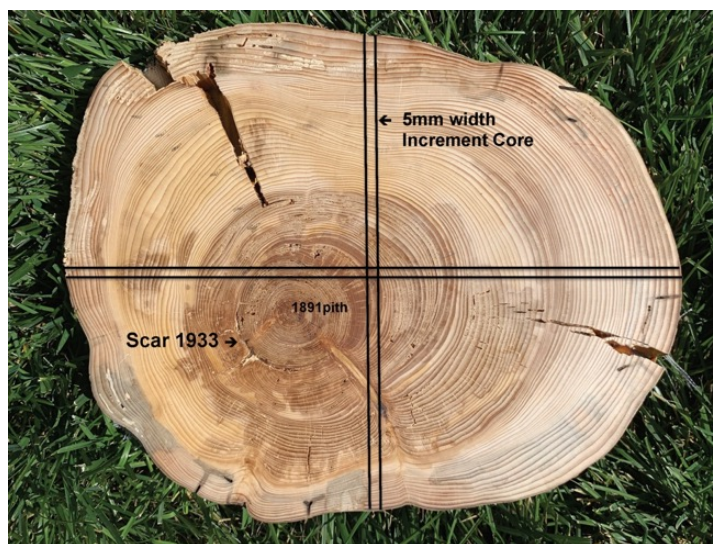


299

300 **Figure 3: Histograms of (a) number of classification of responses, (b) percentage of classification of responses, (c)**
 301 **sample age (red line represents mean age), and (d) species. For species: ABLA=*Abies Lasciocarpa*, PIEN = *Picea***
 302 ***engelmannii*, PSME = *Pseudotsuga menziesii*, THPL = *Thuja plicata*, PICO = *Pinus contorta*, POTR = *Populus***
 303 ***tremuloides*, LARIX = *Larix* Mill., BETUL = *Betula* L., POBA = *Populus balsamifera*.**

304 3.1 Avalanche Event Detection: Cores versus Cross-Sections

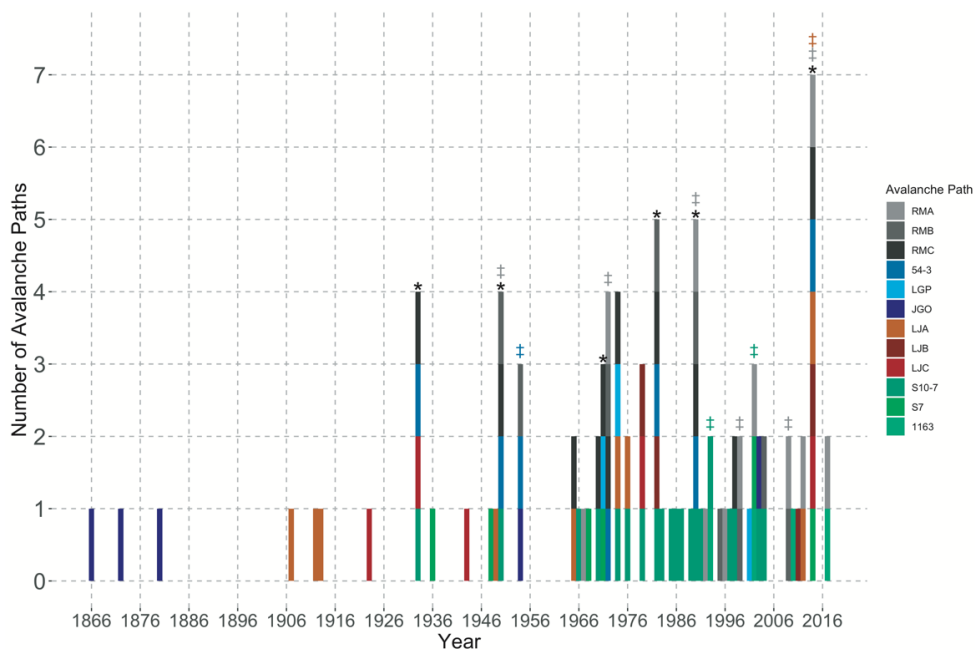
305 The avalanche event subset analysis that compared results obtained as if samples were from cores versus full
 306 cross sections showed that core samples alone would have missed numerous avalanche events and generated
 307 a greater proportion of low-quality growth disturbance classifications (Figure 4). For the subset of 40 samples
 308 analyzed as cores we identified only 124 of 191 (65%) total GD. Of the 66 GDs that we would have missed
 309 just by using cores, 24 were classified as C₁ quality events, 24 were C₂, 14 were C₃, 3 were C₄, and 2 were
 310 C₅.



311
312 **Figure 4:** Example of cross section sample where 4 cores taken on uphill, downhill, and perpendicular (2) would
313 have missed at least one scar (1933) and potentially the pith of the tree. The black lines indicate the potential cores
314 using a 5 mm width increment borer.

315 3.2 Individual Path Chronologies

316 There were 49 avalanche events identified from GD responses across all 12 individual paths in the study
317 region. The avalanche years most common throughout all of the individual path chronologies were: 2014 (7
318 paths); 1982 and 1990 (5 paths); and 1933, 1950, 1972, and 1974 (4 paths) (Figure 5 and Table 4). We
319 identified the year with the greatest number of individual tree GD responses (2002) in 3 paths. Two of these
320 paths were in the JFS sub-region as well as the RMA path in the WF sub-region. There was no clear pattern
321 of paths physically closer in proximity to each other having more similarly identified avalanche years.
322 However, paths within the WF sub-region produced the most similar number of large magnitude avalanche
323 years. When we applied the W_{ii} process step to more heavily weight higher quality signals, the number of
324 identified avalanche years did not change for any individual avalanche path compared to application of the
325 double threshold method alone. This highlights the number of responses classified as C₁ and C₂ (high quality)
326 in our dataset.



327

328 **Figure 5: Number of individual avalanche paths identified per year. Avalanche years with ‡ (gray=WF, dark blue**
 329 **= GTSR, orange = Swan, green= JFS) indicate years identified in at least two avalanche paths in the sub-region.**
 330 *** represents avalanche years in common in at least 1 path from at least three of the four sub-regions.**

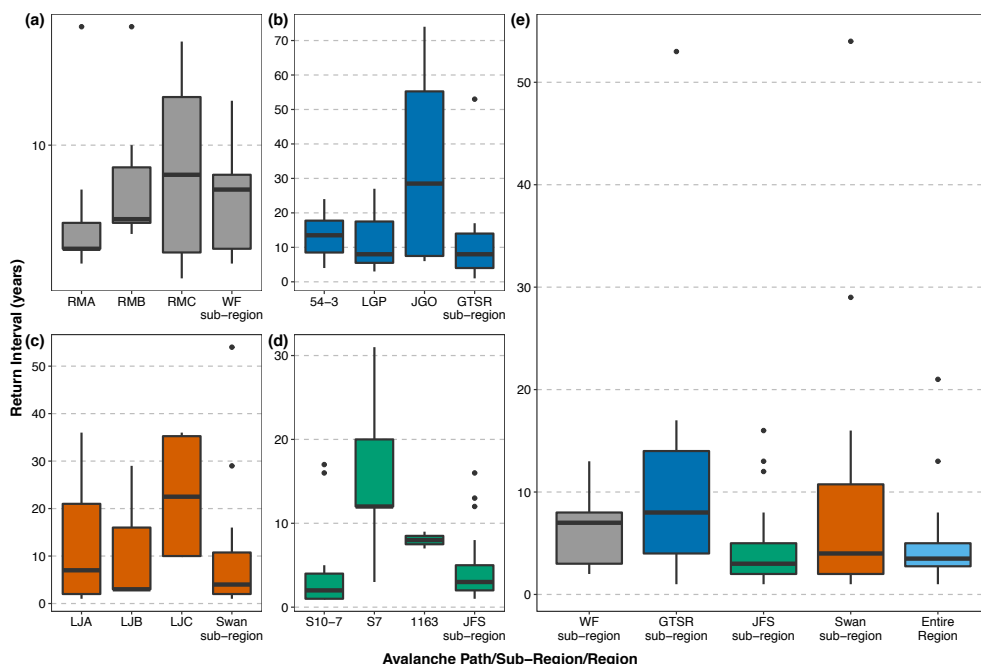
331



332 **Table 4: Avalanche chronologies and return interval (RI) statistics of all 12 avalanche paths in the region.**
 333 **Avalanche years in bold indicate years identified in at least two avalanche paths in the sub-region. Underlined**
 334 **avalanche years indicate years in common in at least 1 path from at least three of the four sub-regions.**

	RMA	RMB	RMC	54-3	LGP	JGO	LJA	LJB	LJC	Shed 10-7	Shed 7	1163
Aval Years	1967 1972 1990 1992 1996 1999 2002 2009 2012 2014 2017	1950 1954 1972 1982 1990 1995 2004 2009	<u>1933</u> 1950 1965 <u>1933</u> 1970 <u>1954</u> 1972 1974 <u>1982</u> <u>1990</u> 1998 2014	<u>1933</u> <u>1950</u> 1954 1972 <u>1982</u> <u>1990</u> 2014	1971 2001 2009	1866 1872 1880 2001 1954 2003	1907 1912 1913 1949 1965 1974 1976 2012 2014	1979 <u>1982</u> 2011 2014	1923 <u>1933</u> 1943 1979 2014	<u>1933</u> <u>1950</u> 1966 1970 1974 1976 1979 <u>1982</u> 1983 1985 1986 1987 1989 <u>1990</u> 1991 1993 1997 1998 2003 2004	1936 1948 1968 <u>1971</u> 2002 2014	1993 2002 2010 2017
# of aval. years	11	9	11	7	4	5	9	4	5	20	6	4
RI median	3	5	8	14	8	8	7	3	22.5	2	12	8
RI - mean	5	7.38	8.1	13.5	12.67	34.25	13.38	11.67	22.75	3.74	15.6	8
RI - min.	2	4	1	4	3	6	1	3	10	1	3	7
RI - max.	18	18	17	24	27	74	36	29	36	17	31	9
1/RI	0.33	0.20	0.13	0.07	0.13	0.13	0.14	0.33	0.04	0.50	0.08	0.13
σ	4.81	4.78	6.12	7.42	12.66	33.09	14.79	15.01	14.73	4.68	10.50	1.00

335
 336 Across all individual paths, the median estimated return interval was 8 years with a range of 2 to 22.5 (Figure
 337 6). JGO, located in the GTSR sub-region, exhibited the greatest spread in estimated return intervals followed
 338 by LJB. The avalanche paths within the GTSR sub-region had the most similar return intervals of any of the
 339 sub-regions whereas the paths in the JFS sub-region exhibited substantial variability in median return interval
 340 values. The return interval for JGO differed significantly from several other paths: RMA, RMB, RMC, and
 341 Shed 10-7 ($p \leq 0.01$). However, when we relax a strict cutoff of $p = 0.05$, the return interval from JGO also
 342 differed from 1163 ($p = 0.07$) and LJA ($p = 0.08$). Similarly, the return interval for Shed 10-7 differs from LJC
 343 ($p = 0.07$). In assessing the potential geomorphic controls on return interval, path length was the only
 344 significantly correlated characteristic ($r = 0.65$, $p = 0.02$, Figure A1).



345
 346 **Figure 6: Boxplot of return intervals for individual avalanche paths in each sub-region: (a) WF, (b) GTSR, (c)**
 347 **Swan, and (d) JFS. (e) shows the median return intervals for the sub-regions and the overall region.**

348 **3.2 Sub-region Chronologies**

349 When the paths were aggregated into sub-regions (three paths per sub-region) the median return periods for
 350 each sub-region were similar and all less than 10 years (Figure 6(e) and Table 5). The number of avalanche
 351 years for all of the sub-regions ranges from 12-18 with the greatest number of identified years in the JFS sub-
 352 region and the fewest in the WF sub-region. The JFS sub-region has the shortest median return interval
 353 followed by the Swan, WF, and GTSR sub-regions. The number of avalanche years for each aggregated sub-
 354 region is greater than the number of avalanche years for any individual path within each sub-region except
 355 for the JFS sub-region where 18 avalanche years were identified but Shed 10-7 totaled 20 avalanche years
 356 (Table 6).

357



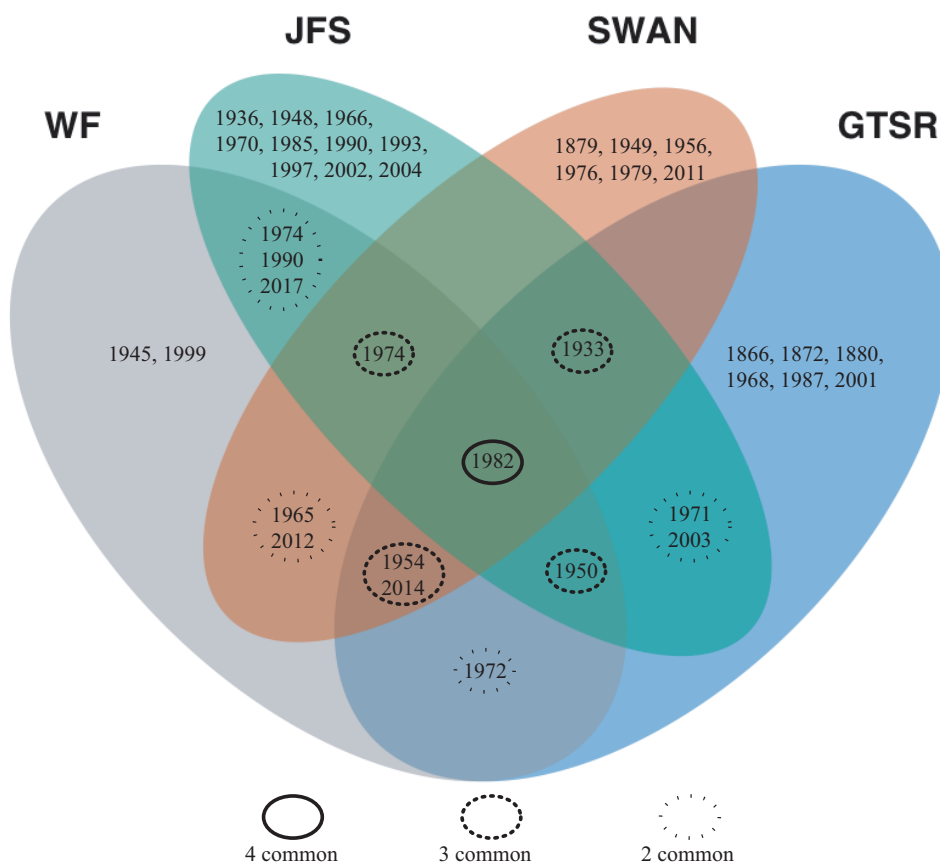
358 **Table 5: Avalanche chronologies and return interval (RI) statistics of all four sub-regions.**

	WF	GTSR	Swan	JFS	Region
# of aval. years	12	14	13	18	30
RI median	7	8	4	3	3
RI – mean	6.27	11.35	11.25	4.94	5.21
RI – min.	2	1	1	1	1
RI – max.	13	53	54	16	53
1/RI	0.14	0.13	0.25	0.33	0.33
σ	3.69	13.48	15.70	4.60	9.53

359
 360 **Table 6: Number of avalanche events for each subregion, the mean of three individual paths in each region, and**
 361 **the overall aggregated region.**

# of avalanche events		
Sub-region	3 individual paths	Aggregated sub-region
WF	11,9,11	12
GTSR	7,3,5	14
Swan	9,4,5	13
JFS	20,6,4	18
Region	30	

362
 363 In terms of commonality of years between the sub-regions, 1982 is the only year identified in all of the four
 364 sub-regions (Figure 7). Avalanche years commonly identified in three sub-regions are 1950, 1954, 1974 and
 365 2014. The JFS sub-region identified the greatest number of years exclusive to that sub-region (10 years). The
 366 WF sub-region shared the greatest number of years with other regions (11 years) followed by JFS (9 years),
 367 GTSR (8 years), and the Swan (7 years). In the only available comparison against an incomplete and limited
 368 historical record, the individual reconstructed avalanche chronologies of paths in the JFS sub-region captured
 369 10-50% of the recorded large magnitude events over years 1908 to 2017.

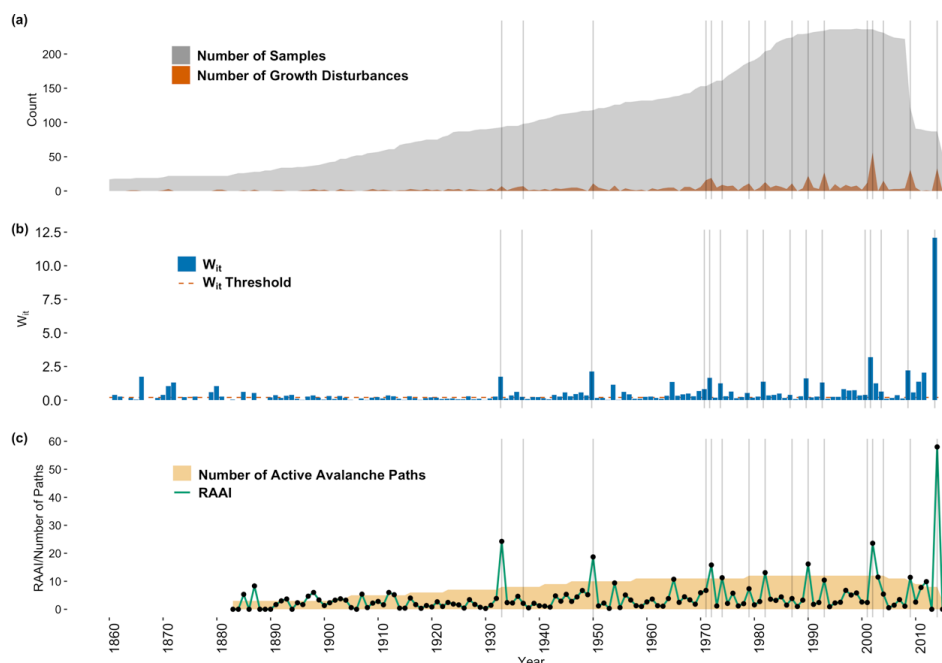


370

371 **Figure 7: Venn diagram of avalanche years common between sub-regions. Overlapping areas of each ellipse**
 372 **indicate years in common with each sub-region.**

373 **3.3 Regional Chronology and RAAI**

374 We identified 30 avalanche years in the overall region and a median return interval of 3 years (Table 5). The
 375 number of samples increases through time to a peak during 2005 and as expected the number of GD also
 376 increases through time (Figure 8(a)). The W_{it} index also increases, particularly from year 2000 onward with
 377 the largest spikes in 2014 and 2017 (Figure 8(b)). The regional assessment of avalanche years identified
 378 fewer years ($n=30$) than the simple aggregation of all unique avalanche years identified in the individual
 379 paths ($n=49$) (Table A2).



380

381 **Figure 8:** (a) The number of samples (gray shaded area) increases through time, but the number of responses
382 (dark orange shaded area) varies. (b) The W_{it} threshold (0.2, red dashed line) provides a means of discriminating
383 between high and low confidence signals in the tree ring record. (c) The RAAI (green line, black points) is a
384 measure of regional avalanche activity based on the I_t of each path and the number of active avalanche paths
385 (yellow shaded area).

386 When we included all paths but S10.7 (one of two paths with the greatest sample size), we captured 80% of
387 all avalanche years and added one new year to the chronology (Table 7). When we removed LGP (the other
388 path with the greatest sample size), we still captured all of the years in the regional chronology but introduced
389 four new years into the chronology for a total of 34 years. A random sample of eight (two from each sub-
390 region) of the 12 avalanche paths captured 83% of the years in the chronology and identified two new
391 avalanche years. Finally, when using only one path from each sub-region with the largest samples size (Shed
392 10-7, 54-3, LJA, and RMA), we captured 73% of the avalanche years identified in the full regional
393 chronology. When using a random sample of one path from each sub-region (1163, LGP, LJC, RMB), we
394 captured only 43% of the years included in the regional chronology of all 12 paths. The RAAI is insensitive
395 (no significant difference, $p > 0.05$) to the number of paths when tested using a minimum number of paths
396 recording an avalanche in year t . The years with the largest RAAI are 2014 and 2017 followed by 2002, 1950
397 and 1933 (Figure 8(c)).

398



399 Table 7: Comparison of the number of avalanche years and RI when including all 12 paths in region to using a
 400 combination of fewer paths to define the region.
 401

Paths	Region (All Paths)	All but S10.7	All but LGP	All but 54-3	S7, 1163, LGP, JGO, RMB, RMC, LJB, LJC	S10.7, 54-3, LJA, RMA	1163, LGP, LJC, RMB
# Paths	12	11	11	11	8	4	4
Sample Size (n)	635	528	526	581	382	253	239
# of Aval Years	30	27	34	31	27	34	17
# matches with regional	NA	24	30	29	25	22	13
# not in regional	NA	1	4	2	2	11	4
% captured in regional	NA	80	100	97	83	73	43
Median RI	3	3	3	3	3	2	3.5
# years removed using only W_{it} =HLC instead of W_{it} =MLC and HLC	10	3	9	7	1	1	1

402
 403 To assess potential long-term trends in regional avalanche activity we implemented the modified Mann-
 404 Kendall test since the chronology exhibits weak serial autocorrelation. The full period of record of RAAI
 405 (1867-2017) exhibits a positive trend ($\tau = 0.186$, Sens slope = -0.01 , $p = 0.006$). The two other periods
 406 analyzed, 1950-2017 and 1990-2017, exhibit neither a positive nor a negative trend ($p = 0.36$ and $p = 0.95$,
 407 respectively).
 408 The probability of detection for the avalanche years (POD_{year}) identified in the regional chronology ranged
 409 from 8 to 58% when we examined individual paths (Table 8). The year with the highest POD was 2014. The
 410 mean POD for all years was 21%. When we examined avalanche paths that exhibited at least one scar during
 411 avalanche years identified in the regional chronologies, the POD is generally greater.
 412



413 Table 8: Probability of Detection (POD_{year}). Avalanche years identified in the regional chronology and associated
 414 POD by analyzing individual paths with and without GD, sample size, and W_i thresholds.

Avalanche Year in Regional Chronology	POD (%) with thresholds	POD (%) without thresholds
1866	8	8
1872	8	8
1880	8	17
1933	33	58
1936	8	25
1945	NA	58
1948	8	33
1950	33	58
1954	25	67
1956	NA	58
1965	17	67
1970	17	50
1971	25	50
1972	33	83
1974	33	75
1976	17	50
1982	42	92
1990	42	83
1993	17	50
1997	8	92
1998	17	50
1999	17	58
2002	25	75
2003	17	33
2004	17	75
2009	17	33
2011	8	33
2012	17	42
2014	58	58
2017	17	25
Mean	21	52

415
 416 Finally, the probability of capturing all of the avalanche years identified in the regional chronology by each
 417 individual path ranges from 7% to 40% (Table 9). The greatest POD_{path} value from any given path is S10.7
 418 ($POD = 40\%$) in the JFS sub-region followed by RMC in the Whitefish sub-region ($POD = 37\%$). In general,
 419 the paths within the Whitefish sub-region capture the regional chronology most consistently.
 420



421 **Table 9: Probability of Detection of each individual path (POD_{path}) to the regional avalanche chronology.**

Path	POD (%)
RMA	27
RMB	27
RMC	37
54-3	23
LGP	7
JGO	17
LJA	17
LJB	10
LJC	7
Shed 10-7	40
Shed 7	17
1163	10

422 **4. Discussion**

423 The processing and analysis of 673 samples spanning a large spatial extent allowed us to create a robust
424 regional large magnitude avalanche chronology reconstructed using dendrochronological methods. Cross-
425 sections provided a more robust and complete GD and avalanche chronology compared to a subsample
426 generated from cores alone. Due to the reduced information value of working only with cores, Favillier et al.
427 (2017) included a discriminatory step in their methods to distinguish avalanche signals in the tree-ring record
428 from exogenous factors, such as abnormal climate signals or response to insect disturbance. By using cross
429 sections to develop our avalanche chronologies, we were able to view the entire ring growth and potential
430 disturbance around the circumference of the tree as opposed to the limited view provided by cores. This
431 allowed us to place GD signals in context to both climate and insect disturbance without the need for this
432 processing step. We identified 2134 GD from our samples, which is similar to Martin and Germain's (2016)
433 study where they collected 458 cross sections and 350 cores, and reported 2251 GD.

434 We targeted sample collection in areas in the runout zones and along the trim line where large magnitude
435 avalanches occurred in recent years. However, at several sites we also collected samples up into the bottom
436 of the track (S10.7, Shed 7, and 1163). Thus, some additional noise in the final chronology for those specific
437 paths could be due to more frequent small magnitude avalanches. Though the oldest individual trees extended
438 as far back as the mid-17th century, the application of the double thresholds and W_{it} processing steps restricted
439 individual path avalanche chronology lengths since the minimum GD threshold requirements were not met.
440 It is difficult to place much confidence in these older recorded events due to the decreasing evidence back in
441 time inherent in avalanche path tree-ring studies. Therefore, we chose to examine more recent time periods
442 with a larger sample size and more consistent number of sites and individual series when considering return
443 intervals and RAAI.

444 All of the paths in the study are capable of producing large magnitude avalanches with path lengths greater
445 than 100 m (typical length for avalanche destructive size 2, D2), and all but RMC have a typical path length
446 of close to or greater than 1000 m (for avalanche destructive size 3, D3) (Greene et al., 2016). As Corona et



447 al. (2012) note, the avalanche event must be large enough to create an impact on the tree, and size D2 or
448 greater will be evident from the tree-ring record (Reardon et al., 2008). However, the successive damage and
449 removal of trees from events size D2 or greater also impacts the future potential to record subsequent events
450 of similar magnitude. In other words, if a large magnitude avalanche removes a large swath of trees in one
451 year, then there are fewer trees available to record a slightly smaller magnitude avalanche in subsequent
452 years. Therefore, dendrochronology methods inherently underestimate avalanche events by up to 60%
453 (Corona et al., 2012), and our results suggest these methods captured about 10-50% of the available historical
454 record for JFS canyon.

455 **4.1 Regional Sampling Strategy**

456 By examining three different spatial scales (individual path, sub-region, and region) we produced a large
457 magnitude avalanche chronology for the region captured in a small subset of the total number of paths across
458 the large region. Accordingly, this sampling strategy may also alleviate the issue of recording large magnitude
459 avalanches within a region in the successive years following a major destructive avalanche event that
460 removed large number of trees within specific paths but not others. Overall, a regional sampling strategy
461 enables us to capture large magnitude avalanche events over a broad spatial extent that is useful for regional
462 avalanche forecasting operations and future climate association analysis. This strategy also allows us to
463 understand large magnitude avalanche activity at scales smaller than the regional scale.

464 **4.2 Chronologies for Individual Paths and Sub-Regions**

465 We applied the W_{it} threshold specifically to weight higher quality signals. The number of identified avalanche
466 years does not change for any individual avalanche path when we applied the W_{it} process. This suggests that
467 many of the signals in our samples were ranked as high-quality (i.e. C₁-C₂). This can be attributed to the use
468 of cross sections which allowed for a more complete depiction and assessment of the tree-ring signal (Carrara,
469 1979).

470 We developed avalanche chronologies for 12 individual avalanche paths. The path with the greatest number
471 of identified avalanche years, S10.7, contains two major starting zones that are both steeper (35 and 39
472 degrees) than Shed 7, which also contains two separate starting zones. Reardon et al. (2008) collected a
473 substantial number of samples at higher elevations in the avalanche path. However, the location data for these
474 samples were not available. Many of those samples were the living stumps that captured smaller annual
475 events. This is likely the root of the difference and the reason S10.7 contains the largest numbers of avalanche
476 years in this analysis.

477 The range of return intervals across all paths (2 – 22.5 years) is similar to those reported for 12 avalanche
478 paths across a smaller spatial extent in the Chic Choc Mountains of Quebec, Canada (2 – 22.8) (Germain et
479 al., 2009). Although the authors in that study used a different avalanche signal index, this still suggests
480 considerable variation in avalanche frequency across avalanche paths within a region.



481 The return intervals for LJC in the Swan sub-region were the greatest and this is likely due to wildfire activity
482 in this path in 2003. LJC was heavily burned, and this created a steep slope with few trees that was once
483 moderately to heavily forested. Substantial anchoring and snowfall interception likely created an avalanche
484 path without many large magnitude avalanches for decades since slope forestation plays a substantial role in
485 runout distance and avalanche frequency in forested areas (Teich et al., 2012). In addition, wildfires in 1910
486 burned a majority of the JFS sub-region as well and the higher frequency of avalanche years recorded between
487 1910 and 1940 in S10.7 suggests this may also be a contributor to the high frequency of avalanche events in
488 that location (Reardon et al., 2008).

489 Our results also suggest that return interval increases as path length increases, though the sample size for this
490 correlation analysis on individual paths is small ($n=12$). This is likely because only large magnitude
491 avalanches affect the far extent of the runout of the path. This differs from a group of avalanche paths in
492 Rogers Pass, British Columbia, Canada, where path length was not significantly correlated with avalanche
493 frequency (Smith and McClung, 1997). However, that study used all observed avalanches, including artillery-
494 initiated avalanches, as opposed to a tree-ring reconstructed dataset.

495 JGO contains the maximum return interval for any path in the study, and the return intervals are significantly
496 different than numerous other paths. A lack of recording data after one large avalanche event could easily
497 skew this value. Another potential explanation is that this path is the only one located east of the Continental
498 Divide where the snowpack is often much shallower, particularly at lower elevations (Selkowitz et al., 2002),
499 thus inhibiting frequent large magnitude events from impacting the sampled runout zone. The fetch upwind
500 of this avalanche path is characterized by steep, rocky terrain harboring scoured slopes. This limits the
501 amount of snow available for transport to the JGO starting zone which may also influence the load and stress
502 placed upon this starting zone and subsequent large magnitude avalanches.

503 The greatest number of identified avalanche years is in the JFS sub-region. The avalanche paths in this sub-
504 region are all south or southeasterly facing whereas the other sub-regions span a greater range of aspects.
505 This may cause a bias toward a more unified representation of that aspect compared to the inclusion of other
506 aspects in the JFS sub-region.

507 The differences between sub-regions are likely due to localized terrain and weather factors and the interaction
508 of the two (Chesley-Preston, 2010). For example, Birkeland (2001) demonstrated significant variability of
509 slope stability across a small mountain range dependent upon terrain and weather. Slope stability and
510 subsequent large magnitude avalanching are likely to be highly heterogeneous across not only the sub-region,
511 but across a large region. This is also consistent with findings by Schweizer et al. (2003) that suggest
512 substantial differences in stability between sub-regions despite the presence of widespread weak layers.

513 **4.3 Regional Chronologies and RAAI**

514 The regional chronology we developed through the use of tree-ring analysis on collections made across 12
515 avalanche paths suggests, unsurprisingly, that the inclusion of more avalanche paths across a large spatial
516 extent produces a more robust identification of major avalanche winters. When we aggregate all 12 paths



517 together and apply established thresholds to discriminate the signal from the noise, we identified 30 avalanche
518 years throughout the region. This allows us to place each year in context of the region, or full extent of the
519 scale triplet, rather than simply collating all of the major avalanche winters identified in each individual path
520 or sub-region. However, we also account for the support and spacing by including adjacent avalanche paths
521 within a sub-region and multiple sub-regions throughout the region. This sampling strategy combined with
522 the large sample size collected throughout the region allowed for a robust assessment of regional avalanche
523 chronology derived from tree-ring records.

524 We tested the sensitivity of the term regional by removing specific and random paths. Our results suggest
525 that removing paths from this structure, and subsequently compromising the sampling strategy, introduces
526 noise. By reducing the sample size, we reduce the ability of the thresholds to filter out noise, thereby
527 increasing the actual number of avalanche years in the region. However, the sample size reduction also
528 reduces the number of identified avalanche winters common to the full 12 path regional record (Table 7).
529 Our results emphasize the importance of sampling more paths spread throughout the region of interest as well
530 as a large dataset across the spatial extent.

531 Avalanche path selection is clearly important when trying to assess avalanche frequency (de Bouchard
532 d'Aubeterre et al., 2019), and this is supported by our results suggesting that S10.7 is more influential than
533 any other path in our study (Table 7). However, selecting multiple paths throughout the region representing
534 a wide range of geomorphic characteristics and potentially influenced by local weather patterns provides a
535 reasonable assessment of regional avalanche activity in areas without historical records. By quantifying the
536 sensitivity of the number of avalanche paths within a given region, we illustrate that sampling a greater
537 number of avalanche paths dramatically increases the probability of identifying more avalanche years as well
538 as increases the ability to reconstruct major avalanche cycle chronologies. However, as previously noted,
539 dendrochronological techniques tend to underestimate avalanche frequency, which implies that caution
540 should be used when interpreting a regional avalanche signal using this technique, particularly as sample
541 numbers and qualities (e.g. cores vs. cross sections) decline.

542 Interestingly, the difference in median return interval throughout the “region” using 12 paths compared to
543 using four or eight paths changes only slightly. This suggests that fewer paths are still able to represent the
544 major avalanche return intervals across a region. However, choosing fewer paths appears to introduce more
545 noise and therefore fewer years identified than a regional chronology with more avalanche paths.

546 The RAAI provides a measure of avalanche activity scaled to the number of active avalanche paths across
547 the region through time. The years with the greatest RAAI value coincide with substantial activity provided
548 in the historical record as well as previous dendrochronological studies from the JFS sub-region (Butler and
549 Malanson, 1985a, b; Reardon et al., 2008). The winter of 1932-33 was characterized by heavy snowfall and
550 persistent cold temperatures leading to extensive avalanche activity that destroyed roadway infrastructure in
551 the JFS sub-region, 1950 saw a nearly month-long closure of U.S. Highway 2 due to avalanche activity, and
552 in 2002, an avalanche caused a train derailment. While these are all confined to the JFS sub-region, with the
553 exception of 2002, they are also years shared by at least two other sub-regions.



554 We examined the probability of detecting an avalanche year throughout the region by sampling any one given
555 path. In seven of 30 years, the POD_{year} is only 8% and in all but three years the POD_{year} is less than 40%. The
556 low POD values are distributed throughout the time series, suggesting decreasing sample size back in time
557 or the number of active avalanche paths is not an influential factor. The POD is likely reflective of the spatial
558 variability of large magnitude avalanche occurrence across a region. It also aligns with the observational
559 findings of Mears (1992). During a major storm in 1986 throughout much of the western United States that
560 deposited 30-60 cm of snow water equivalent, Mears (1992) reports that in the area around Gothic, Colorado
561 less than 40% of avalanche paths produced avalanches and less than 10% produced avalanches approaching
562 the 100-year return interval. This also confirms the wide variability of avalanche years between sub-regions
563 recorded in our tree-ring record. Additionally, some of the avalanches in a given cycle may not be large
564 enough to be reflected in the tree ring record. Therefore, low values of POD_{path} when considering only one
565 avalanche path and identifying only one common year of large magnitude avalanche activity (1982) amongst
566 the sub-regions through dendrochronology is not surprising. Paths with at least one scar (i.e. without applying
567 thresholds) during avalanche years identified in the regional chronology exhibit a greater POD_{path} , but this
568 greater POD_{path} comes at the expense of introducing more noise if we were to simply use one scar per path
569 to define an avalanche event.

570 Our results also suggest that our sampling design using scale triplet increases the probability of detecting
571 avalanche activity across an entire region. We note that we are only able to scale our probability calculations
572 to our dataset with a limited historical observational record. However, our results illustrate the importance of
573 sampling more paths if the goal is to reconstruct a regional chronology. In our dataset, the greatest value of
574 POD_{path} is 40% suggesting that if by chance, we sampled this path we would have captured the regional
575 avalanche activity 40% of the time.

576 The trends in RAAI over the entire period of record are likely influenced by the decreasing number of samples
577 available to record an event further back in time. Despite the RAAI accounting for the number of avalanche
578 paths (minimum of $n = 3$), the small sample size from the late 19th century precludes us from suggesting there
579 is a true increase in regional avalanche activity from 1867 to 2017. This is also supported by the absence of
580 positive or negative trend from 1950 to 2017 and 1990 to 2017.

581 4.4 Limitations

582 Overall, our results strongly suggest that sampling one path, or multiple paths in one sub-region, is
583 insufficient to extrapolate avalanche activity beyond those paths. Multiple paths nested within sub-regions
584 are necessary to glean information regarding avalanche activity throughout those sub-regions as well as the
585 overall region. Our study is still limited by the underrepresentation inherent in dendrochronological
586 techniques for identifying all avalanche events. While we analyzed 673 samples over the extent of the region,
587 some of the paths in our study had relatively small sample sizes per individual path as compared to recent
588 suggestions (Corona et al., 2012). This may have influenced the number of avalanche years identified and
589 subsequent return intervals per individual path. However, we attempted to limit the influence of sample size



590 by using full cross-sections from trees, robust and critical identification of signals in the tree-rings, and
591 appropriate established threshold techniques.

592 We also recognize that sampling more avalanche paths in our region would certainly provide a more robust
593 regional avalanche chronology, but time, cost, and resource constraints required an optimized strategy.
594 Finally, our study would undoubtedly have benefited from a longer and more accurate historical record for
595 comparisons and verification of the tree-ring record in all of the sub-regions. Overall, our study illustrates
596 the importance of considering spatial scale and extent when designing, and making inferences from, regional
597 avalanche studies using tree-ring records.

598 **5. Conclusions**

599 We developed a large magnitude avalanche chronology using dendrochronological techniques for a region
600 in the northern U.S. Rocky Mountains. Implementing a strategic sampling design allowed us to examine
601 avalanche activity through time in single avalanche paths, four sub-regions, and throughout the region. By
602 analyzing 673 samples from 12 avalanche paths, we identified 30 years with large magnitude events across
603 the region and a median return interval of ~3 years. Large magnitude avalanche return interval and number
604 of avalanche years vary throughout the sub-regions, suggesting the importance of local terrain and weather
605 factors. Our work emphasizes the importance of sample size, scale, and spatial extent when attempting to
606 derive a regional large magnitude avalanche chronology from tree-ring records. In our dataset, the greatest
607 value of POD_{path} is 40% suggesting that if we sampled only this path, we would have captured the regional
608 avalanche activity 40% of the time. This clearly demonstrates that a single path cannot provide a reliable
609 regional avalanche chronology. Specifically, our results emphasize the importance of 1) sampling more paths
610 spread throughout the region of interest; 2) collecting a large number of cross-sections relative to cores; and,
611 3) generating a large dataset that scales to the appropriate spatial extent. Future work should include
612 conducting a similar study with a number of paths in the same sub-regions for verification, or in an area with
613 a more robust regional historical record for verification.

614



615 **6. Appendix A**

616 **Table A1: Regional chronologies from the International Tree-Ring Database used for cross-dating.**

MT Avalanche Project Site	ITRDB Tree-Ring Chron.	Originator	Date Range	Species	Coordinates	Elevation	NOAA set ID	data ID
Going-to-the-Sun Road sites	Going to the Sun Road (GTS)	Gregory T. Pederson Jeremy S. Littell	1337 - 2002	PSME	48.42 -113.5167	1860M	noaa-tree-27540_MT15	9
John Stevens Canyon sites	F. Doody Mountain (DOO)	Gregory T. Pederson Blase Reardon	1660 - 2001	PSME	48.3833 -113.6167	1890M	noaa-tree-27536_MT15	5
Lost Johnny Creek sites	Preston Park (PP)	Bekker, M.F.; Tikalsky, B.P.; Fagre, D.B.; Bills, S.D.	1766 - 2006	ABLA	48.43 -113.39	2150M	noaa-tree-5993_MT117	
Red Meadow sites	Numa Ridge Falls (NRF)	Gregory T. Pederson Brian Peters	1645 - 2001	PSME	48.51 -114.12	1695M	noaa-tree-27550_MT16	8

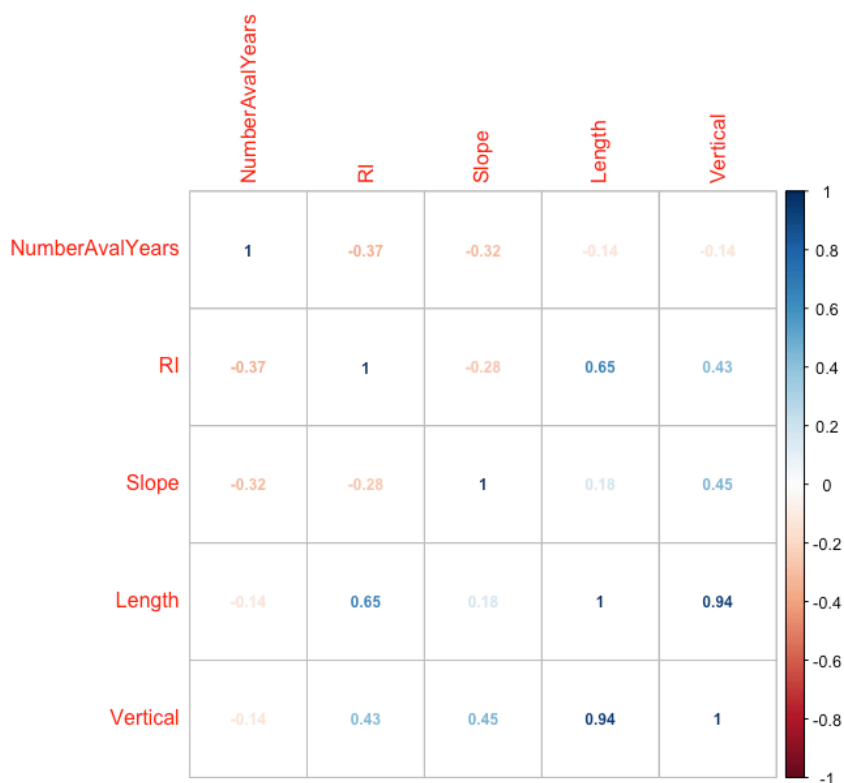
617
 618
 619
 620
 621

Table A2: Avalanche Years identified in the regional analysis (Region, n=29) and avalanche years identified in one or more paths in the individual avalanche path analysis (Ind. Paths Unique Years, n=49). Years in bold indicate years in common between the two sets (n=27).

Region	Ind. Paths Unique Years
1866	1866
1872	1872
1880	1880
	1907
	1912
	1913
	1923
1933	1933
1936	1936
	1943
	1945
1948	1948
	1949
1950	1950
1954	1954
	1956



1965	1965
	1966
	1967
	1968
1970	1970
1971	1971
1972	1972
1974	1974
1976	1976
	1979
1982	1982
	1983
	1985
	1986
	1987
	1989
1990	1990
	1991
	1992
1993	1993
	1995
	1996
1997	1997
1998	1998
	1999
	2001
2002	2002
2003	2003
2004	2004
2009	2009
	2010
2011	2011
2012	2012
2014	2014
2017	2017



623

624 **Figure A1: Correlation matrix (Pearson correlations coefficients) of the number of avalanche years, return**
625 **interval (RI), starting zone slope angle (Slope), and path length (Length).**

626 7. Data availability

627 Data for this work can be found in ScienceBase repository: Peitzsch, E. H., Stahle, D. K., Fagre, D. B., Clark,
628 A. M., Pederson, G. T., Hendrikx, J., and Birkeland, K. W.: Tree ring dataset for a regional avalanche
629 chronology in northwest Montana, 1636-2017. U.S. Geological Survey., U.S. Geological Survey data release,
630 <https://doi.org/10.5066/P9TLHZAI>, 2019.

631 8. Author contribution

632 EP responsible for study conception and design, data collection, analysis, writing. JH contributed to
633 development of study design, methods, editing, and writing. DS responsible for data collection, tree-ring
634 processing and analysis and writing. GP, KB, and DF contributed to study design, editing and writing.



635 **9. Disclaimer**

636 Any use of trade, firm, or product names is for descriptive purposes only and does not imply endorsement by
637 the U.S. Government.

638 **10. Acknowledgements**

639 We extend gratitude to Adam Clark for his substantial data collection efforts and Zach Miller for his
640 assistance processing samples. This work was supported by the USGS Land Resources Western Mountain
641 Initiative project.

642 **11. References**

643 Armstrong, B. R.: A quantitative analysis of avalanche hazard on U.S. Highway 550, southwestern Colorado,
644 in: Proceedings of the Western Snow Conference, St. George, Utah, April 14-16, 2017, 95-104, 1981.

645

646 Ballesteros-Canovas, J. A., Trappmann, D., Madrigal-Gonzalez, J., Eckert, N., and Stoffel, M.: Climate
647 warming enhances snow avalanche risk in the Western Himalayas, Proc. Natl. Acad. Sci. U.S.A., 115, 3410-
648 3415, [10.1073/pnas.1716913115](https://doi.org/10.1073/pnas.1716913115), 2018.

649

650 Bebi, P., Kulakowski, D., and Rixen, C.: Snow avalanche disturbances in forest ecosystems-State of research
651 and implications for management, For. Ecol. and Manage., 257, 1883-1892, [10.1016/j.foreco.2009.01.050](https://doi.org/10.1016/j.foreco.2009.01.050),
652 2009.

653

654 Birkeland, K. W.: Spatial patterns of snow stability throughout a small mountain range, J. Glaciol., 47, 176-
655 186, [10.3189/172756501781832250](https://doi.org/10.3189/172756501781832250) 2001.

656

657 Blöschl, G., and Sivapalan, M.: Scale issues in hydrological modelling: A review, Hydrol. Processes, 9, 251-
658 290, [10.1002/hyp.3360090305](https://doi.org/10.1002/hyp.3360090305) 1995.

659

660 Blöschl, G.: Scaling issues in snow hydrology, Hydrol. Processes, 13, 2149-2175, [10.1002/\(SICI\)1099-
661 1085\(199910\)13:14/15%3C2149::AID-HYP847%3E3.0.CO;2-8](https://doi.org/10.1002/(SICI)1099-1085(199910)13:14/15%3C2149::AID-HYP847%3E3.0.CO;2-8), 1999.

662

663 Bryant, C.L., Butler, D.R., Vitek, J.D.: A statistical analysis of tree-ring dating in conjunction with snow
664 avalanches – comparison of on-path versus off-path responses, Environ. Geol. Water Sci., 14, 53-59,
665 [10.1007/BF01740585](https://doi.org/10.1007/BF01740585), 1989.

666

667



- 668 Burrows, C. J., and Burrows, V. L.: Procedures for the study of snow avalanche chronology using growth
669 layers of woody plants, Institute of Arctic and Alpine Research, University of Colorado, Boulder, CO,
670 Occasional Paper No. 23, 56 pp., 1976.
671
- 672 Butler, D. R.: Snow avalanche path terrain and vegetation, Glacier National Park, Montana, *Arc. and Alp.*
673 *Res.*, 11, 17-32, [10.1080/00040851.1979.12004114](https://doi.org/10.1080/00040851.1979.12004114), 1979.
674
- 675 Butler, D. R., and Malanson, G. P.: A history of high-magnitude snow avalanches, southern Glacier National
676 Park, Montana, U.S.A., *Mt. Res. Dev.*, 5, 175-182, [10.2307/3673256](https://doi.org/10.2307/3673256), 1985a.
677
- 678 Butler, D. R., and Malanson, G. P.: A reconstruction of snow-avalanche characteristics in Montana, U.S.A.,
679 using vegetative indicators, *J. of Glaciol.*, 31, 185-187, [10.3189/S002214300006444](https://doi.org/10.3189/S002214300006444), 1985b.
680
- 681 Butler, D. R., Malanson, G. P., and Oelfke, J. G.: Tree-ring analysis and natural hazard chronologies:
682 minimum sample sizes and index values, *Prof. Geogr.*, 39, 41-47, [10.1111/j.0033-0124.1987.00041.x](https://doi.org/10.1111/j.0033-0124.1987.00041.x), 1987.
683
- 684 Butler, D. R., and Sawyer, C. F.: Dendrogeomorphology and high-magnitude snow avalanches: a review and
685 case study, *Nat. Hazard Earth Sys.*, 8, 303-309, [10.5194/nhess-8-303-2008](https://doi.org/10.5194/nhess-8-303-2008), 2008.
686
- 687 Colorado Avalanche Information Center Statistics and Reporting.
688 <http://avalanche.state.co.us/accidents/statistics-and-reporting/>, last access: June 8, 2020.
689
- 690 Carrara, P. E.: The determination of snow avalanche frequency through tree-ring analysis and historical
691 records, *Geol. Soc. Am. Bull.*, 90, 773-780, [10.1130/0016-7606\(1979\)90%3C773:TDOSAF%3E2.0.CO;2](https://doi.org/10.1130/0016-7606(1979)90%3C773:TDOSAF%3E2.0.CO;2),
692 1979.
693
- 694 Casteller, A., Stoeckli, V., Villalba, R., Mayer, A.C.: An evaluation of dendroecological indicators of snow
695 avalanches in the Swiss Alps, *Arct. Antarct. Alp. Res.*, 39, 218-228, [10.1657/1523-
696 0430\(2007\)39\[218:AEODIO\]2.0.CO;2](https://doi.org/10.1657/1523-0430(2007)39[218:AEODIO]2.0.CO;2), 2007.
697
- 698 Casteller, A., Villalba, R., Araneo, D., and Stöckli, V.: Reconstructing temporal patterns of snow avalanches
699 at Lago del Desierto, southern Patagonian Andes, *Cold Reg. Sci. Technol.*, 67, 68-78,
700 [10.1016/j.coldregions.2011.02.001](https://doi.org/10.1016/j.coldregions.2011.02.001), 2011.
701
- 702 Chesley-Preston, T.: Patterns of natural avalanche activity associated with new snow water equivalence and
703 upper atmospheric wind direction and speed in the mountains surrounding Gothic, Colorado, Master of
704 Science, Department of Earth Sciences, Montana State University, Bozeman, Montana, 75 pp., 2010.



705
706 Corona, C., Lopez Saez, J., Stoffel, M., Bonnefoy, M., Richard, D., Astrade, L., and Berger, F.: How much
707 of the real avalanche activity can be captured with tree rings? An evaluation of classic dendrogeomorphic
708 approaches and comparison with historical archives, *Cold Reg. Sci. Technol.*, 74-75, 31-42,
709 10.1016/j.coldregions.2012.01.003, 2012.
710
711 de Bouchard d'Aubeterre, G., Favillier, A., Mainieri, R., Lopez Saez, J., Eckert, N., Saulnier, M., Peiry, J. L.,
712 Stoffel, M., and Corona, C.: Tree-ring reconstruction of snow avalanche activity: Does avalanche path
713 selection matter?, *Sci. Total Environ.*, 684, 496-508, 10.1016/j.scitotenv.2019.05.194, 2019.
714
715 Dube, S., Filion, L., and Hetu, B.: Tree-Ring Reconstruction of High-Magnitude Snow Avalanches in the
716 Northern Gaspé Peninsula, Quebec, Canada, *Arct. Antarct. Alp. Res.*, 36, 555-564, [10.1657/1523-
717 0430\(2004\)036\[0555:TROHSA\]2.0.CO;2](https://doi.org/10.1657/1523-0430(2004)036[0555:TROHSA]2.0.CO;2), 2004.
718
719 Favillier, A., Guillet, S., Morel, P., Corona, C., Lopez Saez, J., Eckert, N., Ballesteros Cánovas, J. A., Peiry,
720 J.-L., and Stoffel, M.: Disentangling the impacts of exogenous disturbances on forest stands to assess multi-
721 centennial tree-ring reconstructions of avalanche activity in the upper Goms Valley (Canton of Valais,
722 Switzerland), *Quat. Geochronol.*, 42, 89-104, 10.1016/j.quageo.2017.09.001, 2017.
723
724 Favillier, A., Guillet, S., Trappmann, D., Morel, P., Lopez-Saez, J., Eckert, N., Zenhäusern, G., Peiry, J.-L.,
725 Stoffel, M., and Corona, C.: Spatio-temporal maps of past avalanche events derived from tree-ring analysis:
726 A case study in the Zermatt valley (Valais, Switzerland), *Cold Reg. Sci. Technol.*, 154, 9-22,
727 10.1016/j.coldregions.2018.06.004, 2018.
728
729 Germain, D., Filion, L., and Héту, B.: Snow avalanche activity after fire and logging disturbances, northern
730 Gaspé Peninsula, Quebec, Canada, *Can. J. of Earth Sci.*, 42, 2103-2116, 10.1139/c05-087, 2005.
731
732 Germain, D., Filion, L., and Héту, B.: Snow avalanche regime and climatic conditions in the Chic-Choc
733 Range, eastern Canada, *Clim. Change*, 92, 141-167, 10.1007/s10584-008-9439-4, 2009.
734
735 Germain, D., Héту, B., and Filion, L.: Tree-ring based reconstruction of past snow avalanche events and risk
736 assessment in Northern Gaspé Peninsula (Québec, Canada), in: *Tree Rings and Natural Hazards - A State-
737 of-the-Art*, edited by: Stoffel, M., Bollschweiler, M., Butler, D. R., and Luckman, B. H., *Advances in Global
738 Change Research*, Springer, London, 51-73, 2010.
739
740 Google. (n.d.). [Imagery of study area, northwest Montana]. Retrieved February 4, 2020 using R statistical
741 package `get_map`.



742
743 Gratton, M., Germain, D., and Boucher, É.: Meteorological triggering scenarios of tree-ring-based snow
744 avalanche occurrence on scree slopes in a maritime climate, Eastern Canada, *Phys. Geogr.*, 1-18,
745 10.1080/02723646.2019.1573622, 2019.
746
747 Greene, E., Birkeland, K. W., Elder, K., McCammon, I., Staples, M., and Sharaf, D.: Snow, weather, and
748 avalanches: Observation guidelines for avalanche programs in the United States (3rd ed), American
749 Avalanche Association, Victor, ID, 104 pp., 2016.
750
751 Grissino-Mayer, H.: Evaluating crossdating accuracy: A manual and tutorial for the computer
752 program COFECHA, *Tree-Ring Res.*, 57, 205-221, 2001.
753
754 Hamed, K. H., and Rao, A. R.: A modified Mann-Kendall trend test for autocorrelated data, *J. Hydrol.*, 204,
755 182-196, 10.1016/S0022-1694(97)00125-X, 1998.
756
757 Hebertson, E. G., and Jenkins, M. J.: Historic climate factors associated with major avalanche years on the
758 Wasatch Plateau, Utah, *Cold Reg. Sci. Technol.*, 37, 315-332, 10.1016/S0165-232x(03)00073-9, 2003.
759
760 Hendriks, J., Murphy, M., and Onslow, T.: Classification trees as a tool for operational avalanche forecasting
761 on the Seward Highway, Alaska, *Cold Reg. Sci. and Technol.*, 97, 113-120,
762 10.1016/j.coldregions.2013.08.009, 2014.
763
764 Holmes, R. L.: Analysis of tree rings and fire scars to establish fire history, *Tree-Ring Bulletin*, 43, 51-67,
765 1983.
766
767 International Tree Ring Data Bank (ITRDB): [https://www.ncdc.noaa.gov/data-access/paleoclimatology-](https://www.ncdc.noaa.gov/data-access/paleoclimatology-data/datasets/tree-ring)
768 [data/datasets/tree-ring](https://www.ncdc.noaa.gov/data-access/paleoclimatology-data/datasets/tree-ring), access: March 1, 2018.
769
770 Kogelnig-Mayer, B., Stoffel, M., Schneuwly-Bollsweiler, M., Hübl, J., and Rudolf-Miklau, F.:
771 Possibilities and Limitations of Dendrogeomorphic Time-Series Reconstructions on Sites Influenced by
772 Debris Flows and Frequent Snow Avalanche Activity, *Arct. Antarct. Alp. Res.*, 43, 649-658, 10.1657/1938-
773 4246-43.4.649, 2011.
774
775 Korpela, M., Wickham, H., Jackson, S. *ggmap* v3.0.0 – Spatial Visualization with *ggplot2*.
776 <https://github.com/dkahle/ggmap>, 2019.
777



778 Köse, N., Aydın, A., Akkemik, Ü., Yurtseven, H., and Güner, T.: Using tree-ring signals and numerical
779 model to identify the snow avalanche tracks in Kastamonu, Turkey, *Nat. Hazards*, 54, 435-449,
780 10.1007/s11069-009-9477-x, 2010.
781
782 Malevich, S. B., Guiterman, C. H., and Margolis, E. Q.: burnr : Fire history analysis and graphics in R,
783 *Dendrochronologia*, 49, 9-15, 10.1016/j.dendro.2018.02.005, 2018.
784
785 Mann, H. B.: Nonparametric tests against trend, *Econometrica*, 13, 245-259, 10.2307/1907187, 1945.
786
787 Martin, J. P., and Germain, D.: Dendrogeomorphic reconstruction of snow avalanche regime and triggering
788 weather conditions: A classification tree model approach, *Prog. Phys. Geog.*, 10.1177/0309133315625863,
789 2016.
790
791 Mears, A. I.: Snow-Avalanche Hazard Analysis for Land-use Planning and Engineering, Colorado
792 Geological Survey Bulletin, 49, 55 pp., 1992.
793
794 Meseşan, F., Gavrilă, I. G., and Pop, O. T.: Calculating snow-avalanche return period from tree-ring data,
795 *Nat. Hazards*, 94, 1081-1098, 10.1007/s11069-018-3457-y, 2018.
796
797 Mock, C. J., and Birkeland, K. W.: Snow avalanche climatology of the western United States mountain
798 ranges, *Bull. Am. Meteorol. Soc.*, 81, 2367-2392, [10.1175/1520-
799 0477\(2000\)081%3C2367:SACOTW%3E2.3.CO;2](https://doi.org/10.1175/1520-0477(2000)081%3C2367:SACOTW%3E2.3.CO;2), 2000.
800
801 Mock, C. J., Carter, K. C., and Birkeland, K. W.: Some Perspectives on Avalanche Climatology, *Ann. Am.
802 Assoc. of Geogr.*, 1-10, 10.1080/24694452.2016.1203285, 2016.
803
804 Muntan, E., Garcia, C., Oller, P., Marti, G., Garcia, A., and Gutierrez, E.: Reconstructing snow avalanches
805 in the Southeastern Pyrenees, *Nat. Hazard Earth Sys.*, 9, 1599-1612, 10.5194/nhess-9-1599-2009, 2009.
806
807 Ott, R. L., and Longnecker, M. T.: *An Introduction to Statistical Methods and Data Analysis*, 7th Edition ed.,
808 Cengage Learning, Boston, MA, 1296 pp., 2016.
809
810 Peitzsch, E. H., Stahle, D. K., Fagre, D. B., Clark, A. M., Pederson, G. T., Hendriks, J., and Birkeland, K.
811 W.: Tree ring dataset for a regional avalanche chronology in northwest Montana, 1636-2017. U.S. Geological
812 Survey., U.S. Geological Survey data release, 10.5066/P9TLHZAI, 2019.
813



- 814 Pop, O. T., Munteanu, A., Flaviu, M., Gavrilă, I.-G., Timofte, C., and Holobăcă, I.-H.: Tree-ring-based
815 reconstruction of high-magnitude snow avalanches in Piatra Craiului Mountains (Southern Carpathians,
816 Romania), *Geografiska Annaler: Series A, Phys. Geogr.*, 100, 99-115, [10.1080/04353676.2017.1405715](https://doi.org/10.1080/04353676.2017.1405715),
817 2018.
818
- 819 Potter, N.: Tree-ring dating of snow avalanche tracks and the geomorphic activity of avalanches, Northern
820 Absaroka Mountains, Wyoming, *Geol. S. Am. S., Special Paper 123*, 141-165, 1969.
821
- 822 Rayback, S. A.: A dendrogeomorphological analysis of snow avalanches in the Colorado Front Range, USA,
823 *Phys. Geogr.*, 19, 502-515, [10.1080/02723646.1998.10642664](https://doi.org/10.1080/02723646.1998.10642664), 1998.
824
- 825 Reardon, B. A., Pederson, G. T., Caruso, C. J., and Fagre, D. B.: Spatial reconstructions and comparisons of
826 historic snow avalanche frequency and extent using tree rings in Glacier National Park, Montana, U.S.A.,
827 *Arct. Antarct. Alp. Res.*, 40, 148-160, [10.1657/1523-0430\(06-069\)\[REARDON\]2.0.CO;2](https://doi.org/10.1657/1523-0430(06-069)[REARDON]2.0.CO;2), 2008.
828
- 829 Schläppy, R., Jomelli, V., Grancher, D., Stoffel, M., Corona, C., Brunstein, D., Eckert, N., and Deschatres,
830 M.: A New Tree-Ring-Based, Semi-Quantitative Approach for the Determination of Snow Avalanche
831 Events: use of Classification Trees for Validation, *Arct. Antarct. Alp. Res.*, 45, 383-395, [10.1657/1938-4246-
832 45.3.383](https://doi.org/10.1657/1938-4246-45.3.383), 2013.
833
- 834 Schläppy, R., Eckert, N., Jomelli, V., Stoffel, M., Grancher, D., Brunstein, D., Naaim, M., and Deschatres,
835 M.: Validation of extreme snow avalanches and related return periods derived from a statistical-dynamical
836 model using tree-ring techniques, *Cold Reg. Sci. Technol.*, 99, 12-26, [10.1016/j.coldregions.2013.12.001](https://doi.org/10.1016/j.coldregions.2013.12.001),
837 2014.
838
- 839 Schläppy, R., Jomelli, V., Eckert, N., Stoffel, M., Grancher, D., Brunstein, D., Corona, C., and Deschatres,
840 M.: Can we infer avalanche-climate relations using tree-ring data? Case studies in the French Alps, *Reg.
841 Environ. Change*, 16, 629-642, [10.1007/s10113-015-0823-0](https://doi.org/10.1007/s10113-015-0823-0), 2015.
842
- 843 Schweizer, J.: Snow avalanche formation, *Reviews of Geophysics*, 41, [10.1029/2002rg000123](https://doi.org/10.1029/2002rg000123), 2003.
844
- 845 Schweizer, J., Kronholm, K., and Wiesinger, T.: Verification of regional snowpack stability and avalanche
846 danger, *Cold Reg. Sci. and Technol.*, 37, 277-288, [10.1016/s0165-232x\(03\)00070-3](https://doi.org/10.1016/s0165-232x(03)00070-3), 2003.
847
- 848 Selkowitz, D. J., Fagre, D. B., and Reardon, B. A.: Interannual variations in snowpack in the Crown of the
849 Continent Ecosystem, *Hydrol. Process.*, 16, 3651-3665, [10.1002/hyp.1234](https://doi.org/10.1002/hyp.1234), 2002.
850



- 851 Shroder, J. F.: Dendrogeomorphological analysis of mass movement on Table Cliffs Plateau, Utah,
852 Quaternary Res., 9, 168-185, 10.1016/0033-5894(78)90065-0, 1978.
853
- 854 Šilhán, K., and Tichavský, R.: Snow avalanche and debris flow activity in the High Tatras Mountains: New
855 data from using dendrogeomorphic survey, Cold Reg. Sci. Technol., 134, 45-53,
856 10.1016/j.coldregions.2016.12.002, 2017.
857
- 858 Skøien, J. O., and Blöschl, G.: Sampling scale effects in random fields and implications for environmental
859 monitoring, Environ. Monit. Assess., 114, 521-552, 10.1007/s10661-006-4939-z, 2006.
860
- 861 Smith, L.: Indication of snow avalanche periodicity through interpretation of vegetation patterns in the North
862 Cascades, Washington , in: Methods of Avalanche Control on Washington Mountain Highways: Third
863 Annual Report, Washington State Highway Commission Department of Highways, Olympia, Washington,
864 USA, 187 pp., 1973.
865
- 866 Smith, M. J., and McClung, D. M.: Avalanche frequency and terrain characteristics at Rogers' pass, British
867 Columbia, Canada, J. Glaciol., 43, 165-171, [10.3189/S0022143000002926](https://doi.org/10.3189/S0022143000002926), 1997.
868
- 869 Stokes, M. A., and Smiley, T. L.: An Introduction to Tree-Ring Dating, The University of Arizona Press,
870 Tucson, 1996.
871
- 872 Teich, M., Bartelt, P., Grêt-Regamey, A., and Bebi, P.: Snow Avalanches in Forested Terrain: Influence of
873 Forest Parameters, Topography, and Avalanche Characteristics on Runout Distance, Arct. Antarct. Alp. Res.,
874 44, 509-519, 10.1657/1938-4246-44.4.509, 2012.
875
- 876 Voiculescu, M., Onaca, A., and Chiroiu, P.: Dendrogeomorphic reconstruction of past snow avalanche events
877 in Bâlea glacial valley–Făgăraș massif (Southern Carpathians), Romanian Carpathians, Quatern. Int., 415,
878 286-302, 10.1016/j.quaint.2015.11.115, 2016.
879